

# Thermodynamic properties and shear viscosity over entropy density ratio of nuclear fireball in a quantum-molecular dynamics model

C. L. Zhou,<sup>1,2</sup> Y. G. Ma\*,<sup>1</sup> D. Q. Fang,<sup>1</sup> and G. Q. Zhang<sup>1</sup>

<sup>1</sup>*Shanghai Institute of Applied Physics, Chinese Academy of Sciences, Shanghai 201800, China*

<sup>2</sup>*University of Chinese Academy of Sciences, Beijing 100049, China*

(Dated: August 8, 2018)

Thermodynamic and transport properties of nuclear fireball created in the central region of heavy-ion collisions below 400 MeV/nucleon are investigated within the isospin-dependent quantum molecular dynamic (IQMD) model. These properties including the density, temperature, chemical potential, entropy density ( $s$ ) and shear viscosity ( $\eta$ ), are calculated by a generalized hot Thomas Fermi formalism and a parameterized function, which was developed by Danielewicz. As the collision goes on, a transient minimal  $\eta/s = 5/4\pi - 10/4\pi$  occurs in the largest compression stage. Besides, the relationship of  $\eta/s$  to temperature ( $T$ ) in the freeze-out stage displays a local minimum which is about 9-20 times  $1/4\pi$  around  $T = 8-12$  MeV, which can be argued as indicative of a liquid gas phase transition. In addition, the influences of nucleon-nucleon (NN) cross section ( $\sigma_{NN}$ ) and symmetry energy coefficient ( $C_s$ ) are also discussed, and it is found that the results are sensitive to  $\sigma_{NN}$  but not to  $C_s$ .

PACS numbers: 25.70.-z, 21.65.Mn

## I. INTRODUCTION

In the past decades, extensive experimental and theoretical efforts have been devoted to search for the nuclear liquid-gas phase transition (LGPT) in intermediate energy heavy-ion collisions (HIC) [1–12]. Many probes have been suggested for the onset of nuclear LGPT. For instance, the fragment size distribution [13] and its rank distribution [12], the largest fluctuation of the heaviest fragment [14], caloric curve [4, 6], bimodality [15] etc. In addition, it has been observed that the ratio of shear viscosity to entropy density ( $\eta/s$ ) reaches its local minimum at the transition temperature for a wide class of systems. For instance, empirical observation of the temperature or incident energy dependence of the shear viscosity to entropy density ratio for  $\text{H}_2\text{O}$ , He and Ne2 exhibits a minimum in the vicinity of the critical point for phase transition [16]. And a lower bound of  $\eta/s > 1/4\pi$  obtained by Kovtun-Son-Starinets (KSS) for infinitely coupled super-symmetric Yang-Mills gauge theory based on the AdS/CFT duality conjecture, is speculated to be valid universally [17, 18]. In ultra-relativistic HIC [19–23], people have used the ratio of shear viscosity to entropy density to study the quark-gluon plasma phase and the extracted value of  $\eta/s$  seems close to the KSS bound ( $1/4\pi$ ).

So far there are many interesting investigations on the ratio of  $\eta/s$ , but it is still rare to study the behavior of  $\eta/s$  during the heavy-ion collision at intermediate energies [24–27]. Furthermore, the influences of nucleon-nucleon cross section and nuclear symmetry energy are less discussed.

In this work we use a microscopic transport model known as the isospin-dependent quantum dynamics model [28] to simulate Au+Au central collisions. In order to study the effect of nucleon-nucleon cross section, 0.5 times and 1.5 times normal nucleon-nucleon cross section are also used in the simulation. On the other hand for the symmetry energy which is important for asymmetric nuclear matter as well as nuclear astrophysics [29–31], different symmetry energy parameters are employed, namely 15 MeV, 25 MeV and 35 MeV. The generalized hot Thomas Fermi formalism (GHTFF) [32–34] and the transport formula [35] are employed, respectively, to extract thermodynamic and transport properties of the nuclear fireball which is located in the central region with a moderate volume. Then different correlations between the extracted thermal and transport properties are discussed and a good agreement with our previous calculations is found [36]. Furthermore the multiplicity of intermediate mass fragments (IMFs) is also checked as a signal of liquid gas phase transition [37–40] to verify the calculated result.

The paper is organized as follows. Section 2 provides a brief introduction for the IQMD model, GHTFF as well as transport formula for shear viscosity. In Section 3 we present the calculation results and discussions, where the time evolution of thermodynamic quantities and shear viscosity over entropy density are focused. Finally a summary and outlook is given.

## II. MODEL AND FORMULISM

### A. Quantum Molecular Dynamics Model

The quantum molecular dynamics (QMD) [41, 42] model approach is a many-body theory which describes heavy ion collisions from intermediate to relativistic en-

---

\*Author to whom all correspondence should be addressed: ygma@sinap.ac.cn

ergy. The isospin-dependent quantum molecular (IQMD) [42, 43] model is based on the QMD model, including the isospin effects and Pauli blocking. Each nucleon in the colliding system is described as a Gaussian wave packet, i.e.

$$\psi_i(\mathbf{p}_i, \mathbf{r}_i, t) = \frac{1}{(2\pi L)^{3/4}} \exp\left[\frac{i}{\hbar} \mathbf{p}_i(t) \cdot \mathbf{r} - \frac{(\mathbf{r} - \mathbf{r}_i(t))^2}{4L}\right]. \quad (1)$$

Here  $\mathbf{r}_i(t)$  and  $\mathbf{p}_i(t)$  are the mean position and mean momentum, and the Gaussian width has the fixed value  $L = 2.16 \text{ fm}^2$  for Au + Au system. The centers of these Gaussian wave packets propagate in coordinate ( $\mathbf{R}$ ) and momentum ( $\mathbf{P}$ ) space according to the classical equations of motion:

$$\dot{\mathbf{p}}_i = -\frac{\partial \langle \mathbf{H} \rangle}{\partial \mathbf{r}_i}; \quad \dot{\mathbf{r}}_i = \frac{\partial \langle \mathbf{H} \rangle}{\partial \mathbf{p}_i}, \quad (2)$$

where  $\langle \mathbf{H} \rangle$  is the Hamiltonian of the system.

The Wigner distribution function for a single nucleon density in phase space is given by

$$f_i(\mathbf{r}, \mathbf{p}, t) = \frac{1}{(\pi\hbar)^3} \exp\left[\frac{-(\mathbf{r} - \mathbf{r}_i(t))^2}{2L}\right] \exp\left[\frac{-2L(\mathbf{p} - \mathbf{p}_i(t))^2}{\hbar^2}\right]. \quad (3)$$

The mean field in IQMD model is written as

$$U(\rho) = U_{\text{Sky}} + U_{\text{Coul}} + U_{\text{Yuk}} + U_{\text{sym}}, \quad (4)$$

where  $U_{\text{Sky}}$ ,  $U_{\text{Coul}}$ ,  $U_{\text{Yuk}}$ , and  $U_{\text{sym}}$  represents the Skyrme potential, the Coulomb potential, the Yukawa potential and the symmetry potential interaction, respectively [41]. The Skyrme potential is

$$U_{\text{Sky}} = \alpha(\rho/\rho_0) + \beta(\rho/\rho_0)^\gamma, \quad (5)$$

where  $\rho_0 = 0.16 \text{ fm}^{-3}$  and  $\rho$  is the nuclear density. In the present work, the parameters  $\alpha = -356 \text{ MeV}$ ,  $\beta = 303 \text{ MeV}$ , and  $\gamma = 7/6$ , correspond to a soft EOS, are used.  $U^{\text{Yuk}}$  is a long-range interaction (surface) potential, and takes the following form

$$U^{\text{Yuk}} = (V_y/2) \sum_{i \neq j} \exp(Lm^2)/r_{ij} \cdot [\exp(mr_{ij}) \text{erfc}(\sqrt{L}m - r_{ij}/\sqrt{4L}) - \exp(mr_{ij}) \text{erfc}(\sqrt{L}m + r_{ij}/\sqrt{4L})], \quad (6)$$

with  $V_y = 0.0074 \text{ GeV}$ ,  $m = 1.25 \text{ fm}^{-1}$ ,  $L = 2.16 \text{ fm}^2$ , and  $r_{ij}$  is the relative distance between two nucleons. The symmetry potential is  $U_{\text{sym}} = C_s \frac{\rho_n - \rho_p}{\rho_0}$ , where  $\rho_n$ ,  $\rho_p$ , and  $\rho_0$  are the neutron, proton and nucleon densities, respectively.  $C_s$  is the symmetry energy coefficient, and three different values of 15, 25 and 35 MeV are taken in order to study its influence on the ratio of  $\eta/s$ .

Furthermore the isospin degree has entered into the cross sections, which is similar to the parametrization of VerWest and Arndt, see Ref. [44]. The cross section for the neutron-neutron collisions is assumed to be equal to the proton-proton cross sections. In order to study the effect of cross section on the ratio of  $\eta/s$ , the nucleon-nucleon cross section is multiplied by a coefficient  $C_\sigma$ . Three different situations are considered, namely  $C_\sigma$  equals 0.5, 1.0 and 1.5 respectively. In a practical viewpoint, a smaller  $C_\sigma$  seems suitable to describe HIC, which was proposed in the previous work Ref. [45]

$$\sigma_{NN} = C_\sigma \sigma_{NN}^{\text{free}}. \quad (7)$$

From Eq. (3) one obtains the matter density of coordinate space by the sum over all the nucleons, namely

$$\begin{aligned} \rho(\mathbf{r}, t) &= \sum_{j=1}^{A_T+A_P} \rho_j(\mathbf{r}, t) \\ &= \sum_{j=1}^{A_T+A_P} \frac{1}{(2\pi L)^{3/2}} \exp\left[-\frac{(\mathbf{r} - \mathbf{r}_i(t))^2}{2L}\right]. \end{aligned} \quad (8)$$

The kinetic energy density in coordinates space could also be calculated from Eq.(4) by

$$\rho_K(\mathbf{r}, t) = \sum_{j=1}^{A_T+A_P} \frac{\mathbf{P}_j(t)^2}{2m} \rho_j(\mathbf{r}, t). \quad (9)$$

## B. The Generalized Hot Thomas-Fermi Formalism

Thermodynamical properties of hot nuclear matter formed in heavy ion collisions, e.g. temperature and entropy density, can be extracted by using the approach developed by Faessler and collaborators [32–34, 46, 47]. In this approach one starts from a microscopic picture of two interpenetrating pieces of nuclear matter and deduces the thermal quantities from the matter density and kinetic energy density obtained during the collisions. In this paper, the extraction of thermal properties of the hot nuclear matter is done in two steps. First, based on the IQMD simulation, one could calculate the nuclear matter and kinetic energy densities at each point in coordinate space at every time step. Second, by employing the hot Thomas-Fermi formalism, we could obtain the corresponding thermal properties for every set of nuclear matter density and nuclear kinetic energy density [32, 33]. In GHTFF, the momentum distribution in cylindrical coordinates  $k_r, k_z$  can be written as

$$n(K) = \begin{cases} n1(K) = \\ n2(K) = \end{cases} \begin{cases} (1 + \exp[\hbar^2(k_r^2 + k_z^2)/2mT - \mu'_1])^{-1}, & k_z < k_0 \\ (1 + \exp[\hbar^2(k_r^2 + (k_z - k_R)^2)/2mT - \mu'_2])^{-1}, & k_z > k_0 \end{cases}$$

with  $\mu'_i = \mu_i/T$  is the reduced chemical potential,  $k_0 = [k_R^2 - 2mT(\mu'_1 - \mu'_2)]/2k_R$ ,  $k_R$  is the relative momentum between the projectile (index 1) and target (index 2). The local nuclear matter density  $\rho_i$  is expressed as

$$\rho_i = \frac{1}{2}\rho_0(\mu'_i) + \frac{1}{2\pi^2}\left(\frac{2mT}{\hbar^2}\right)^{3/2} \times [f(\mu'_i, K_{0i}) + J_{1/2}(\mu'_i, K_{0i}^2)], \quad (10)$$

where  $K_{01} = \frac{\hbar k_0}{\sqrt{2mT}}$ ,  $K_{02} = K_R - K_{01}$  with  $K_r = \frac{\hbar k_R}{\sqrt{2mT}}$ , and  $J_n(\mu', z) = J_n(\mu', \infty)$  is the Fermi integrals, i.e.

$$J_n(\mu', z) = \int_0^z \frac{x^n dx}{1 + \exp(x - \mu')},$$

$$f(\mu'_i, K_{0i}) = K_{0i} \ln[1 + \exp(\mu'_i - K_{0i}^2)].$$

The local kinetic energy density  $\epsilon = \frac{\hbar^2 \tau_i}{2m}$ , where  $\tau_i$  reads

$$\begin{aligned} \tau_i &= \frac{1}{2}\tau_0(\mu'_i) + \frac{1}{2\pi^2}\left(\frac{2mT}{\hbar^2}\right)^{5/2} \\ &\times \left[ \frac{1}{3}K_{0i}^2 f(\mu'_i, K_{0i}) + \frac{1}{3}J_{1/2}(\mu'_i, K_{0i}^2) \right. \\ &\left. + \int_0^{K_{0i}} J_1(\mu'_i - x^2) dx \right] + \Delta\tau_i(\mu'_i). \end{aligned} \quad (11)$$

And the entropy density  $s_i$  is written as

$$\begin{aligned} s_i &= \frac{1}{2}s_0(\mu'_i) + \frac{1}{2\pi^2}\left(\frac{2mT}{\hbar^2}\right)^{3/2} \\ &\times \left[ \left( \frac{1}{3}K_{0i}^2 - \mu'_i \right) f(\mu'_i, K_{0i}) + \frac{1}{3}J_{1/2}(\mu'_i, K_{0i}^2) \right. \\ &\left. - \mu'_i J_{1/2}(\mu'_i, K_{0i}^2) + 2 \int_0^{K_{0i}} J_1(\mu'_i - x^2) dx \right]. \end{aligned} \quad (12)$$

Here  $i = 1, 2$  represents the projectile and target, and  $\Delta\tau_1(\mu'_1) = 0$ ,

$$\begin{aligned} \Delta\tau_2(\mu'_2) &= \frac{1}{2\pi^2}\left(\frac{2mT}{\hbar^2}\right)^{5/2} K_R \\ &\times [J_1(\mu'_2) - J_1(\mu'_2, K_{02}^2) - K_{02} f(\mu'_2, K_{02})] \\ &+ k_R^2 \rho_2(\mu'_2), \end{aligned}$$

From the Eq.(10,11,12), one can obtain the thermal properties by inversion in principle. But such an inversion procedure is practically not feasible due to the complexity of the equations. Therefore, a more practical way is chosen to obtain the thermal properties. First, we generate all reasonable combinations  $T$ ,  $K_R$  and  $\mu'_i$ , which ranging from 0-100MeV, 0-5  $fm^{-1}$  and 0-2, respectively. Then the corresponding  $\rho_i$ ,  $\tau_i$ ,  $s_i$  could be obtained. Second, from the extracted  $\rho_i$ ,  $\tau_i$  in the central region at each time step during the evolution of collision,  $T$ ,  $K_R$  and  $\mu'_i$  are obtained from the calculations in the first step. Third, the entropy density is calculated according to Eq.12. One should pay attention that all the values displayed in the following pictures are the average one in the central region.

### C. Shear Viscosity Formalism

For largely equilibrated systems, fluxes of macro quantities, leading to dissipation, are proportional to gradients within the system. The shear viscosity denoted as  $\eta$  is the coefficient of proportionality between anisotropy of momentum-flux tensor, including dissipation and velocity gradients [48]. In the Boltzmann statistical limit the shear viscosity corresponds to the first order Chapman-Enskog coefficients. In Ref. [35, 45] the nuclear shear viscosity for normal N-N cross section, has been derived from the microscopic Boltzmann-Uehling-Ulenbeck equation and can be parameterized as a function of density  $\rho$  and temperature  $T$ :

$$\begin{aligned} \eta\left(\frac{\rho}{\rho_0}, T\right) &= \frac{1700}{T^2}\left(\frac{\rho}{\rho_0}\right)^2 + \frac{22}{1 + T^2 10^{-3}}\left(\frac{\rho}{\rho_0}\right)^{0.7} \\ &+ \frac{5.8\sqrt{T}}{1 + 160T^{-2}}, \end{aligned} \quad (13)$$

where  $\eta$  is in MeV/fm<sup>2</sup>c,  $T$  in MeV, and  $\rho_0 = 0.168 \text{fm}^{-3}$ . Figure 1 shows  $\eta$  as a function of  $T$  and  $\rho/\rho_0$ . One can see that  $\eta$  exhibits a very distinct minimum when nuclear matter density is less than normal nuclear density. And as the density increases, the transition temperature also get larger, e.g. for normal density the transition temperature locates around 10 MeV, but for 2.5 times normal density it is almost 50 MeV. This conclusion is coincident with macroscopic result. And in the case of scaled N-N cross section, the shear viscosity just only needs to be scaled by  $\frac{1}{C_\sigma}$ , i.e.

$$\eta\left(\frac{\rho}{\rho_0}, T, C_\sigma\right) = \frac{\eta\left(\frac{\rho}{\rho_0}, T\right)}{C_\sigma} \quad (14)$$

From Eq.14 we can see that the shear viscosity is very sensitive to the N-N cross section, the larger the cross section is, the smaller the shear viscosity. And it is intuitive that large N-N cross section makes the transport of particle momentum much difficult. Since the equilibrium of the considered nuclear matter at the very starting stage is not reached, the calculated shear viscosity should be considered as the transport properties of largely equilibrated nuclear matter with the same density and kinetic energy density.

### III. CALCULATION AND DISCUSSION

In present work, we simulate head-on collision of Au + Au at different beam energies. The reason why we choose the central collision is that the participant zone is the maximal and the matter is more nuclear liquid-like during the early time evolution of collision.

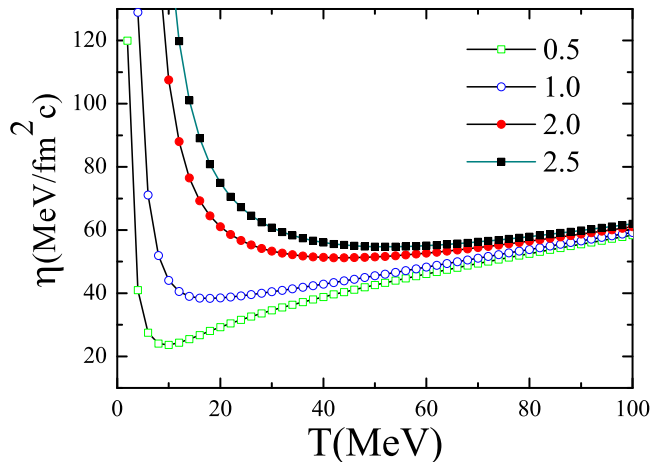


FIG. 1: (Color online) Shear viscosity of nuclear matter as a function of  $\rho/\rho_0$  and  $T$  with the Eq.(13). Different colors represent different  $\rho/\rho_0$ , which are illustrated in the inset.

### A. Time evolution of density profile in reaction plane

Fig. 2 shows the evolution of density profile in X-Z plane for Au+Au head-on collisions at 50 MeV/nucleon and 200 MeV/nucleon at 2, 10, 20, 30, 50 and 80 fm/c. The zero point of time is set at the initial contact between project and target (the first left panel). With the collision goes on, the system overlaps and seems more isotropic in phase space. In order to calculate the thermodynamic quantities in different time steps, we select the central sphere with radius  $r=5$  fm, which defines a volume of nuclear fireball in this paper.

### B. Time evolution of thermodynamic variables

The time evolution of the average nuclear matter density (panel (a)) and kinetic energy density (panel (b)) in the central region, with  $C_\sigma = 1.0$ , is showed in Fig. 3. It is interesting that the maximum density reached is about  $1.5\rho_0$  to  $2.0\rho_0$  and the maximum kinetic energy density is  $10 \text{ MeV fm}^{-3}$  to  $25 \text{ MeV fm}^{-3}$  for the energy displayed in the picture. Along the time scale of the collision one can see that both  $\rho/\rho_0$  and  $\tau$  are reaching their maxima at about 20 fm/c and at a bit earlier time for higher energy. After the compression stage the matter starts to expand and some of them will escape from the central region, mainly in the transverse plane, the matter density drops to very small values and the central region is cooled down. In general the warm and dense nuclear matter survives much longer when the incident energy is low. At about 80 fm/c the hot and dense matter disappears.

Time evolution of matter density and kinetic energy density are shown in Fig. 4, when  $C_\sigma$  and  $C_s$  are set by

different values. The upper panels demonstrate the different cross section situation ( $C_\sigma \in [0.5, 1.0, 1.5]$ ), on the other hand the bottom panels are for different symmetry energy. In panels (a) and (b), it is easy to find that the nuclear matter density and kinetic energy density are different from each other when  $C_\sigma$  is different. We found that there is no difference for the nuclear matter density during compression stage. But when the system starts to expand, the larger nucleon-nucleon cross section makes the dense matter stay longer. In contrast with the behavior of density around the maximum compression stage, more distinction for the kinetic energy density is exhibited. It shows that the smaller the nucleon-nucleon cross section, the larger the kinetic energy density. But these curves almost overlap each other after 40 fm/c, it may be understood that the longitudinal energy enters the central region more easily when the nucleon-nucleon cross section is small. It should be noted that the large kinetic energy density does not mean higher temperature, since the kinetic energy is not calculated in the center of mass frame, detailed information can be found in Refs. [32–34, 46, 47]. In addition, the extracted density and kinetic energy density show insensitivity to the symmetry energy as depicted in panel (c) and (d). The curves are overlapped with each other for the whole process. As has been discussed in the previous paragraph, this leads the nuclear matter to the same thermal properties. So the extracted thermal properties based upon the hot Thomas-Fermi formulism keep exactly the same with each other. So in this paper we just investigate the nucleon-nucleon cross section effect on thermodynamic and transport quantities in the following texts.

Time evolution of temperature is plotted in Fig. 5. Fig. 5(a) shows the time evolution of temperature with  $C_\sigma=1.0$  at different incident energies. Fig. 5(b) shows the time evolution of temperature when the incident energy is fixed at 130 MeV/nucleon but with different cross sections. The following pictures are arranged with the same mode, i.e panel (a) represents a constant cross section  $C_\sigma=1.0$  but at different incident energies; panel (b) means a constant incident energy at 130 MeV/nucleon with different cross sections. For a given beam energy, temperature increases at first, then reaches a local maximum about 20 fm/c and decreases till a saturated value at about 80 fm/c. The higher the incident energy, the larger the maximum value. The corresponding time at maximum value is a little earlier than that for the density and kinetic density. In panel (b), it is found that the larger cross section makes the system a little hotter. The reason is that there are more frequent nucleon-nucleon collisions as  $\sigma_{NN}$  becomes larger, which makes the translation from the longitudinal energy to thermal energy more efficiently.

Fig. 6 shows the time evolution of chemical potential ( $\mu$ ). Again, the left panel displays the normal cross section one, we can find that  $\mu$  increases in the compression stage and decreases in the expansion stage, and the lower the incident energy, the larger the chemical po-

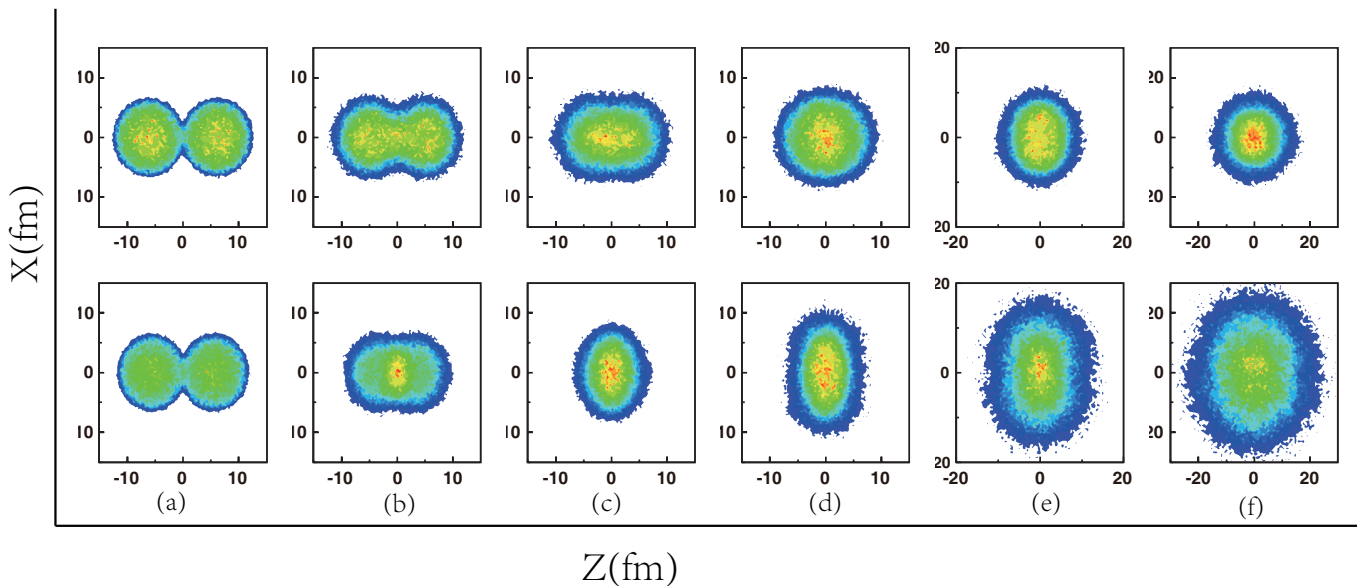


FIG. 2: (Color online) X-Z density profile in different time step for Au+Au head-on collisions at 50 MeV/nucleon (upper panels) and 200 MeV/nucleon (lower panels), respectively. From left to right panels, time step is 2, 10, 20, 30, 50 and 80 fm/c, respectively.

tential. This might be understood as a large compound nucleus is formed during the compression stage, and the lower the incident energy, the larger the compound nucleus is. In panel (b), it shows that the chemical potential becomes generally larger when nucleon-nucleon cross section is larger.

Time evolution of entropy density is plotted in Fig. 7. It is found that the entropy density almost synchronically evolves with the temperature. The higher the incident energy and nucleon-nucleon cross section, the larger the entropy density is.

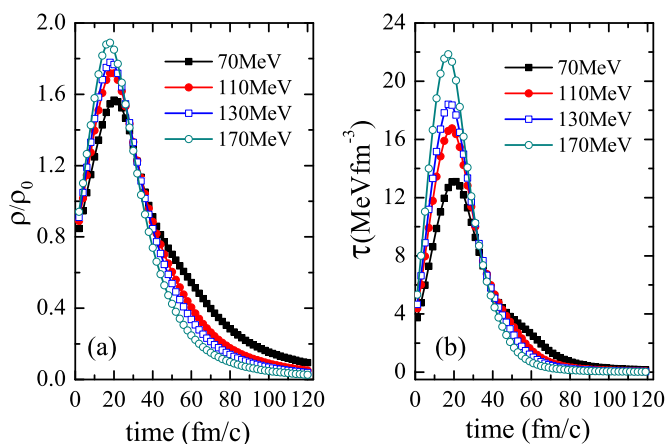


FIG. 3: (Color online) Time evolution of mean matter density (a) and kinetic energy density (b) at different beam energies.

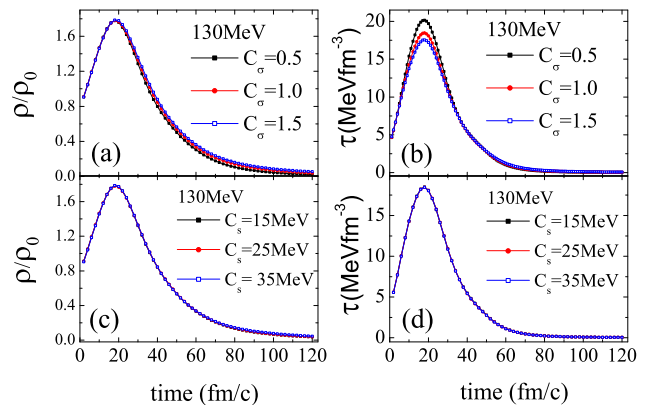


FIG. 4: (Color online) Time evolution of mean nuclear matter density ((a) and (c)), and the kinetic energy density ((b) and (d)) in the central region defined as a sphere with radius equals 5 fm of head-on Au+Au collisions at 130 MeV/nucleon. Different nucleon-nucleon cross section ((a) and (b)) and symmetry energy parameter ((c) and (d)) are used.

### C. Ratio of shear viscosity to entropy density

Now we can move to the discussion on transport coefficient. Since the nuclear participant in central region could be seen as nuclear fluid, we adopt the Eq. 13 to calculate the shear viscosity. Unlike the Green-Kubo formula [27, 48], the advantage of the equation is that we can investigate the time evolution of shear viscosity in the framework of transport model. But it should be noted that Eq. 13 is principally applicable when the sys-

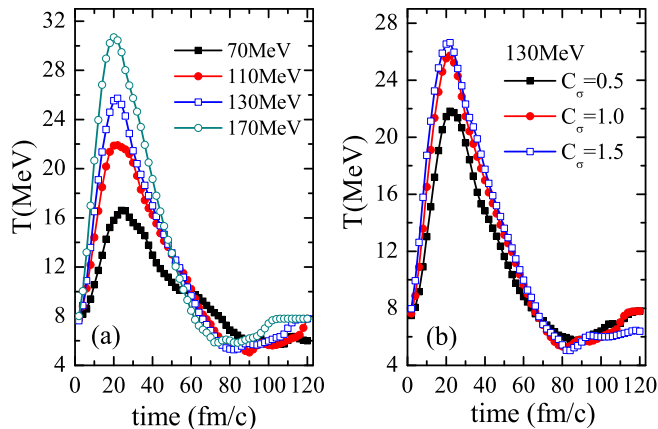


FIG. 5: (Color online) Time evolution of temperature inside the central region at normal nucleon-nucleon cross section at different incident energies (a), or at 130 MeV/nucleon but with different  $\sigma_{NN}$  (b). The incident energies and N-N cross section parameters are illustrated in the inset.

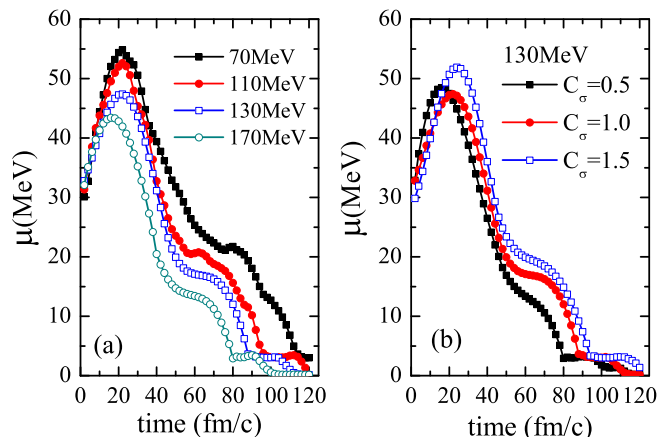


FIG. 6: (Color online) Same as Fig. 5 but for chemical potential.

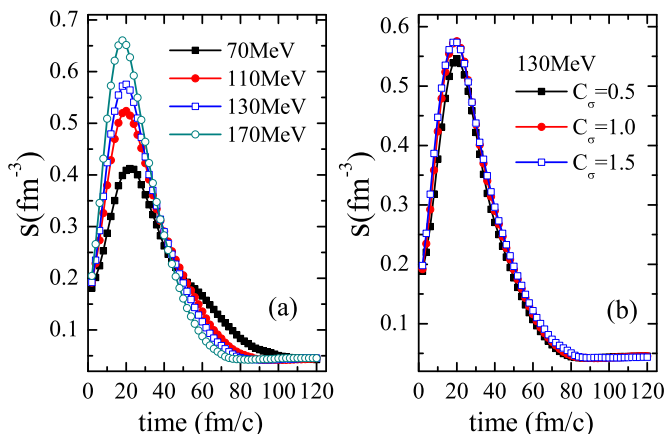


FIG. 7: (Color online) Same as Fig. 5 but for entropy density.

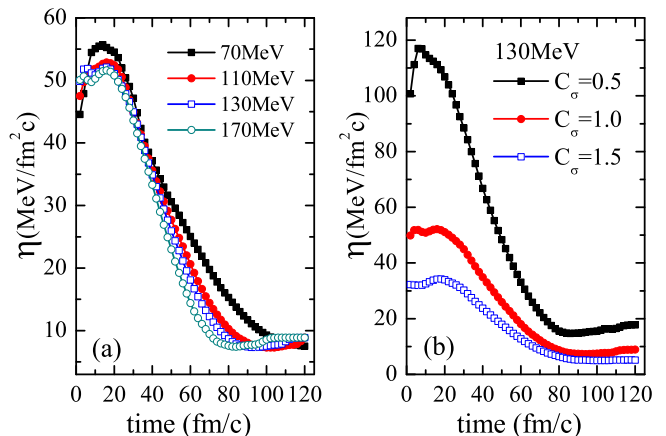


FIG. 8: (Color online) Same as Fig. 5 but for shear viscosity  $\eta$  of the central fireball.

tem is largely equilibrated. However, a full equilibrium is hardly achieved during the whole heavy-ion collision process. So the shear viscosity extracted here should be seen as the properties of an equilibrated nuclear fireball with the same thermodynamic state as the simulated one.

Fig. 8 displays the time evolution of shear viscosity ( $\eta$ ), it shows an increase in earlier stage and then drops with time. As Eq. 1 shows, here the shear viscosity depends on both temperature and density which vary with time. Roughly speaking, the shear viscosity increases in the compression stage and decreases as the system expands. The smaller the nucleon-nucleon cross section, the larger the viscosity in the maximum compression stage. Fig. 8(b) shows that there is a big enhancement when the N-N cross section is scaled by  $C_\sigma = 0.5$ , which is demonstrated in Eq.14, the smaller the N-N cross section the larger the viscosity is.

When the entropy density is taken into account, the ratio of shear viscosity to entropy density shows a minimum near maximum compression point as shown in Fig. 9. From the hydrodynamical point of view, the less the  $\eta/s$ , the more perfect the matter looks like. In this sense, the nuclear matter becomes a more ideal-like liquid around the most compressible point in comparison with other evolution stages. But note that this minimum  $\eta/s$  is just a transient process. In addition, the extent of approaching an ideal-like liquid of the nuclear matter is growing up with the increasing of beam energy. In relativistic energy domain, the  $\eta/s$  of quark-gluon matter becomes very small, close to  $1/4\pi$  (KSS bound), it is called a perfect liquid.

Temperature dependence of  $\eta/s$  is an important issue to understand the transport properties of the nuclear matter in different hot and dense environment. To this end, we plot a correlation between  $\eta/s$  and temperature in Fig. 10(a) at different energies. Note that the density is not fixed in each curve. It is found that there is a decrease of  $\eta/s$  at first when the system is in the com-

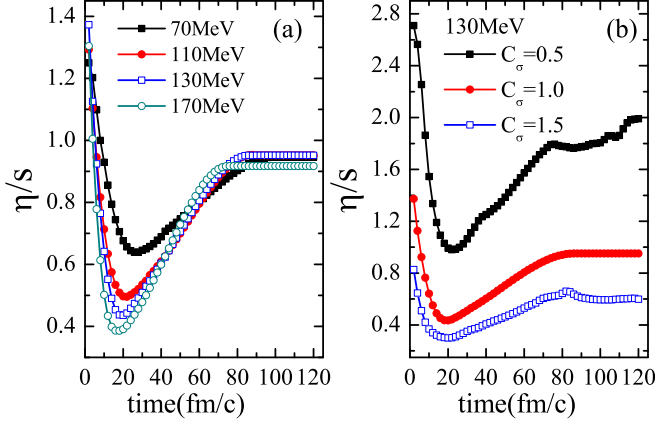


FIG. 9: (Color online) Same as Fig. 5 but for the ratio of shear viscosity to entropy density  $\eta/s$  of the central nuclear fireball.

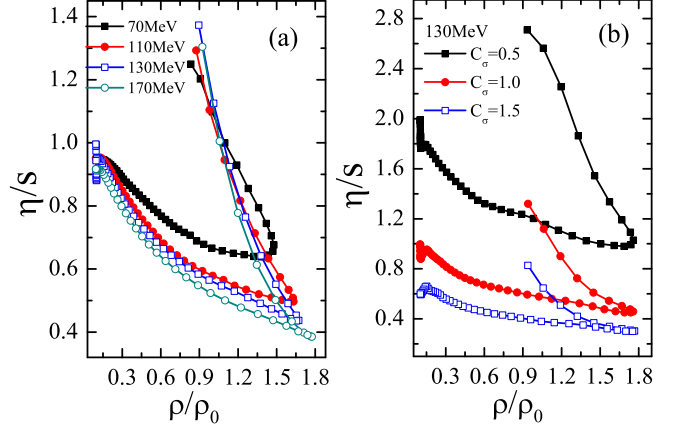


FIG. 11: (Color online) Same as Fig. 10 but for density dependence of  $\eta/s$ .

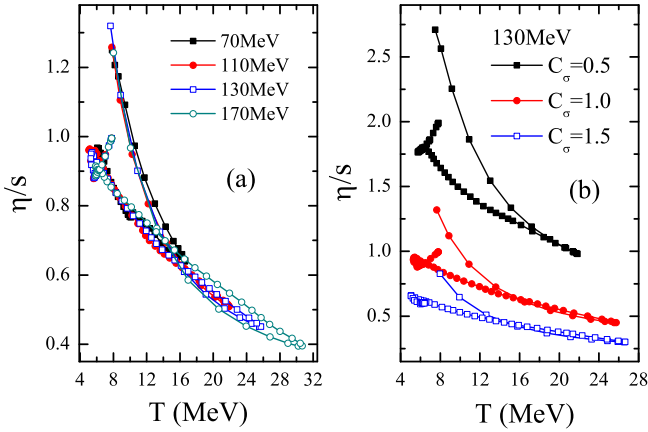


FIG. 10: (Color online) (a): The correlation between  $\eta/s$  and temperature at different beam energies with a normal nucleon-nucleon cross section parametrization; (b): the  $\eta/s$  evolves versus temperature at 130 MeV/nucleon with the different nucleon-nucleon cross section. The incident energy and nucleon-nucleon cross section is illustrated in the inset of (a) and (b), respectively.

pression stage. However,  $\eta/s$  becomes increasing as the system begins to expand. The higher the beam energy, the hotter the nuclear matter, and the smaller the  $\eta/s$ . From this picture it is obvious to find the time when the  $\eta/s$  approaches its transient minimum, essentially corresponds that the nuclear matter reaches the highest temperature. On the other hand, in the present beam energy domain below 400 MeV/nucleon, the transient minimum of  $\eta/s$  which corresponds to the larger compression stage is around 0.4, which is about 5 times of KSS bound (i.e.  $1/4\pi$ ).

Furthermore, we can also extract the correlation between  $\eta/s$  and nuclear matter density as shown in Fig. 11. Here temperature is another hidden variable. Similar to Fig. 10,  $\eta/s$  first drops to a minimum value as the den-

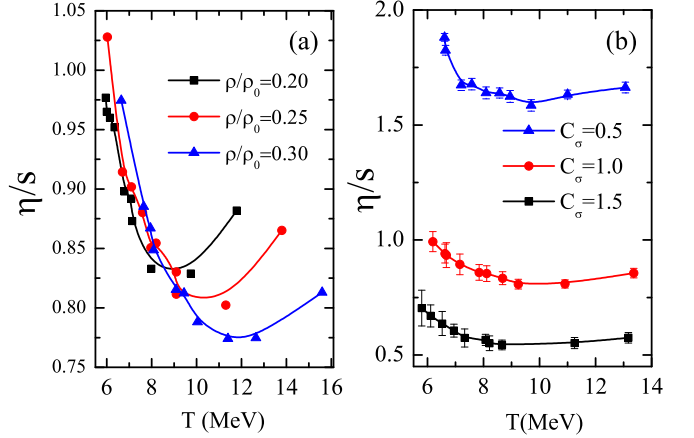


FIG. 12: (Color online) The average of  $\eta/s$  as a function of temperature at different fixed freeze-out densities (a) and different cross sections (b).

sity is compressed to a maximum point and then rises up when the system expands. Larger compressible state produces a less  $\eta/s$ , i.e. the system is close to a more ideal-like state.

Considering that only final reaction products can be detected in experiments, such as the multiplicity and flows of the fragments and light particles, it is therefore necessary to check the  $\eta/s$  in the freeze-out stage and see if it is a useful probe to study the properties of nuclear matter as well as liquid gas phase transition. The freeze-out volume has been already studied in some previous works [49, 50], but in our case, it is more suitable to define a freeze-out density instead. The time average values of  $\eta/s$  when the nuclear matter is in some given freeze-out density regions of  $\rho/\rho_0$  in [0.19, 0.21], [0.24, 0.26] and [0.29, 0.31] have been extracted as a function of temperature.

Fig. 12 shows a correlation of the above average  $\eta/s$  versus temperature for given freeze-out densities (a) and with different  $\sigma_{NN}$  (b). From Fig. 12(a) we observe that there exhibits a local minimum of  $\eta/s$  with a value of 0.76 to 0.84 (about 9-10 times of KSS bound), depending on the freeze-out density, in the range of 8 - 12 MeV of temperature, this phenomenon shall be related to the liquid gas phase transition. With the increasing of freeze-out density, we observe the minimal value of  $\eta/s$  decreases and while its corresponding turning temperature increases. The former is consistent with the results showed in Fig. 12 and the latter can be understood by the transition temperature/pressure increases with the freeze-out density as expected by the pressure-density phase diagram [1, 51]. In contrast with the sensitivity of  $\eta/s$  to freeze-out density, Fig. 12(b) demonstrates that the time averaged  $\eta/s$  when the system is in a given  $\rho/\rho_0$  [0.2, 0.3] is also very sensitive to the  $\sigma_{NN}$ . The larger the N-N cross section is, the smaller the  $\eta/s$  is, which means the nuclear matter behaves much more similar as an ideal fluid.

In order to check the result of  $\eta/s$ , another signal of liquid gas phase transition, namely intermediate mass fragment, is also studied. The intermediate mass fragment which is defined as charge number  $Z \in [3, Z_{total}/3]$ , where  $Z_{total}$  is the total charge number. These fragments are larger than typical evaporated light particles and smaller than the residues and fission products, and they can be considered as nuclear fog. So the multiplicity of intermediate mass fragments ( $M_{IMFs}$ ) is intimately related with the occurrence of liquid gas phase transition. Usually the  $M_{IMFs}$  increases first as the collision system changes toward gas phase, and reaches a maximum, then decreases when the system becomes vaporized [37].

The result of  $M_{IMFs}$  as a function of temperature is showed in Fig. 13. In panel (a), it is interesting to find that the higher the density, the lower the transition temperature is, where the maximum of  $M_{IMFs}$  approaches. This trend is just coincident with the result of  $\eta/s$ , which showed in Fig. 12(a) except the exact value of the transition temperature; In  $M_{IMFs}$  case, the transition temperature  $T \in [7, 10]$ , a little smaller than the  $\eta/s$ 's, where  $T \in [8, 12]$ . The difference could be explained as the nuclear matter is hotter in the central region, so we argue that the minimum of the  $\eta/s$  could be a probe of liquid gas phase transition. In panel (b) the average value of  $M_{IMFs}$  as a function of the average temperature when the nuclear matter density  $\rho \in [0.2, 0.3]\rho_0$ , it is found that the multiplicities of the intermediate mass fragment increase as the N-N cross section is large. This can be understood as large N-N cross section increases the probability of intermediate mass clusters formation. Furthermore, the transition temperature is also increase as the N-N cross section just like the results of Fig. 12(b).

It is interesting to note that phase transition temperature 8 – 12 MeV which corresponds a local minimum of  $\eta/s$  is basically coincident with previous works [52, 53].

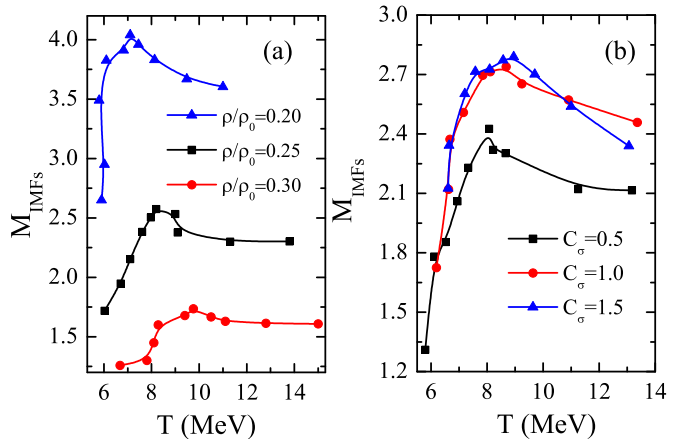


FIG. 13: (Color online) The average of  $M_{IMFs}$  as a function of temperature at different fixed freeze-out density stages (a); the average  $M_{IMFs}$  on the whole freeze out stage with  $\rho/\rho_0 \in [0.2, 0.3]$  as a function of temperature at different cross sections at the (b).

#### IV. SUMMARY AND OUTLOOK

Thermodynamical and transport properties of a fireball formed in head-on Au+Au collisions are investigated in a framework of quantum molecular dynamics model. The relationships between different thermodynamic quantities are explored. The influences of nucleon-nucleon cross section and symmetry energy on the thermodynamical and transport properties are also focused. We found that all the properties are very sensitive to the nucleon-nucleon cross section and insensitive to the symmetry energy. In our calculations, the shear viscosity is calculated by a parametrization formula developed by Danielewicz and entropy density is obtained by a generalized hot Thomas Fermi formalism. The present work gives a time evolution of shear viscosity over entropy density ratio of nuclear fireball, which shows that a transient minimal  $\eta/s$  occurs in the largest compression stage. The results at different beam energies show that the larger the compression, the more ideal the nuclear fireball behaves like fluid. In the present beam energy domain below 400 MeV/nucleon, this transient  $\eta/s$  approaches to 5 times KSS bound.

In addition, temperature and density dependencies of  $\eta/s$  are also investigated. It is of very interesting to observe that a local  $\eta/s$  minimum, which is about 9-20 times KSS bound, emerges from the temperature dependence of  $\eta/s$  at different constant freeze-out densities (0.2 - 0.3  $\rho_0$ ), which corresponds to a liquid-gas phase transition occurring in the intermediate energy heavy-ion collisions. And the larger the N-N cross section, the smaller the  $\eta/s$  is, which means the nuclear matter behaves more like the ideal fluid. From the temperature dependence of  $\eta/s$ , we learn that the phase transition temperature rises up with the freeze-out density. In order to check the result of  $\eta/s$ , another liquid gas phase transition signal,



the multiplicity of the intermediate mass fragment is also checked, and a very nice coincidence is found.

Finally, we like to point out that the present work is still in a phenomenological level for investigating  $\eta/s$  of hot nuclear matter which is formed in intermediate energy heavy-ion collisions, experimental measurements of  $\eta/s$  are still not available so far. Therefore, proposals for direct probes of shear viscosity and entropy density in intermediate energy HIC are very crucial and welcome for constraining the transport properties of nuclear matter around the liquid-gas phase transition.

## ACKNOWLEDGMENTS

This work is partially supported by the NSFC under contracts No. 11035009, 11220101005, 10979074, 11175231, the Major State Basic Research Development Program in China under Contract No. 2013CB834405, and the Knowledge Innovation Project of Chinese Academy of Sciences under Grant No. KJCX2-EW-N01.

- 
- [1] S. Das Gupta, A. Z. Mekjian, and M. B. Tsang, *Adv. Nucl. Phys.* **26**, 89 (2001).
- [2] A. Bonasera, M. Bruno, C. O. Dorso, and P. F. Mastinu, *Riv. Nuovo Cimento* **23**, 1 (2000).
- [3] B. Borderie, M. F. Rivet, *Progr. Part. Nucl. Phys.* **61**, 551 (2008).
- [4] J. Pochodzalla *et al.* (ALADIN Collaboration), *Phys. Rev. Lett.* **75**, 1040 (1995).
- [5] Y. G. Ma *et al.*, *Phys. Lett. B* **390**, 41 (1997).
- [6] J. B. Natowitz, K. Hagel, Y. G. Ma, M. Murray, L. Qin, R. Wada, and J. Wang, *Phys. Rev. Lett.* **89**, 212701 (2002).
- [7] D. H. E. Gross, *Rep. Prog. Phys.* **53**, 605 (1990).
- [8] J. P. Bondorf, A.S. Botvina *et al.*, *Phys. Rep.* **257**, 133 (1995).
- [9] Y. G. Ma, W. Q. Shen, *Nucl. Sci. Tech.* **15**, 4 (2004); G. Q. Zhang *et al.*, *Nucl. Sci. Tech.* **23**, 61 (2012).
- [10] M. L. Gilkes *et al.*, *Phys. Rev. Lett.* **73**, 1590 (1994).
- [11] J. B. Elliott *et al.*, *Phys. Rev. C* **49**, 3185 (1994); *Phys. Rev. Lett.* **88**, 042701 (2002).
- [12] Y. G. Ma, *Phys. Rev. Lett.* **83**, 3617 (1999); *Eur. Phys. J. A* **30**, 227 (2006); Y.G. Ma *et al.*, *Phys. Rev. C* **69**, 031604(R) (2004); *Phys. Rev. C* **71**, 054606 (2005);
- [13] M. E. Fisher, *Rep. Prog. Phys.* **30**, 615 (1969); *Physics* **3**, 255 (1967).
- [14] F. Gulminelli and M. D'Agostino, *Eur. Phys. J. A* **30**, 253 (2006).
- [15] O. Lopez and M.F. Rivet, *Eur. Phys. J. A* **30**, 263 (2006).
- [16] L. P. Csernai, J.I. Kapusta and L.D. McLerran, *Phys. Rev. Lett.* **97**, 152303 (2006).
- [17] P. K. Kovtun, D. T. Son and A. O. Starinets, *Phys. Rev. Lett.* **94**, 111601 (2005).
- [18] G. Policastro, D. T. Son, and A. O. Starinets, *Phys. Rev. Lett.* **87**, 081601 (2001).
- [19] N. Demir, S. A. Bass, *Phys. Rev. Lett.* **102**, 172302 (2009).
- [20] R. Lacey *et al.*, *Phys. Rev. Lett.* **98**, 092301 (2007).
- [21] Jiunn-Wei Chen, Eiji Nakano, *Phys. Lett. B* **647**, 371 (2007).
- [22] J. I. Kapusta and T. Springer, *Phys. Rev. D* **78**, 066017 (2008).
- [23] A. Majumder, B. Müller, and Xin-Nian Wang, *Phys. Rev. Lett.* **99**, 192301 (2007).
- [24] L. Shi and P. Danielewicz, *Phys. Rev. C* **68**, 064604 (2003).
- [25] S. Pal, *Phys. Lett. B* **684**, 211 (2010); *Phys. Rev. C* **81**, 051601(R) (2010).
- [26] N. Auerbach, S. Shlomo, *Phys. Rev. Lett.* **103**, 172501 (2009).
- [27] S. X. Li, D. Q. Fang, Y. G. Ma, C. L. Zhou, *Phys. Rev. C* **84**, 024607 (2011); *Nucl. Sci. Tech.* **22**, 235 (2011).
- [28] Y. G. Ma, *et al.*, *Phys. Rev. C* **73**, 014604 (2006); J. Wang *et al.*, *Nucl. Sci. Tech.* **24**, 030501 (2013); C. Tao *et al.*, *Nucl. Sci. Tech.* **24**, 030502 (2013).
- [29] J. M. Lattimer and M. Prakash, *Science* **304**, 536 (2004); D. T. Loan, N. H. Tan, D. T. Khoa, and J. Margueron, *Phys. Rev. C* **83**, 065809 (2011).
- [30] J. B. Natowitz *et al.*, *Phys. Rev. Lett.* **104**, 202501 (2010); L. Qin *et al.*, *Phys. Rev. Lett.* **108**, 172701 (2012).
- [31] S. Kumar, Y. G. Ma, *Phys. Rev. C* **86**, 051601 (2012); S. Kumar, Y. G. Ma, G. Q. Zhang, and C. L. Zhou, *Phys. Rev. C* **84**, 044620 (2011); **85**, 024620 (2012).
- [32] D. T. Khoa, N. Ohtsuka, A. Faessler, M. A. Matin, S. W. Huang, E. Lehmann and Y. Lotfy, *Nucl. Phys. A* **542**, 671 (1992).
- [33] D. T. Khoa, N. Ohtsuka, A. Faessler, M. A. Matin, S. W. Huang, E. Lehmann and P. K. Puri, *Nucl. Phys. A* **548**, 102 (1992).
- [34] P. K. Puri, N. Ohtsuka, E. Lehmann, A. Faessler, D. T. Khoa, M. A. Matin, G. Batko and S. W. Huang, 1992 GSI Scientific Report 93-1, GSI, Darmstadt, Germany, p. 126.
- [35] P. Danielewicz, *Phys. Lett. B* **146**, 168 (1984).
- [36] C. L. Zhou, Y. G. Ma, D. Q. Fang, *EPL* **98**, 66003 (2011).
- [37] Y. G. Ma, W. Q. Shen, *Phys. Rev. C* **51**, 710 (1995).
- [38] G. F. Peaslee *et al.*, *Phys. Rev. C* **49**, R2271 (1994).
- [39] C. A. Ogilvie *et al.*, *Phys. Rev. Lett.* **67**, 1214 (1991).
- [40] M. B. Tsang *et al.*, *Phys. Rev. Lett.* **71**, 1502 (1993).
- [41] J. Aichelin, *Phys. Rep.* **202**, 233 (1991).
- [42] C. Hartnack, Rajeev K. Puri, J. Aichelin, J. Konopka, S.A. Bass, H. Stöcker, and W. Greiner, *Eur. Phys. J. A* **1**, 151 (1998).
- [43] C. Hartnack, Li Zhuxia, L. Neise, G. Peilert, A. Rosenhauer, H. Sorge, J. Aichelin, H. Stöcker and W. Greiner, *Nucl. Phys. A* **495**, 303c (1989).
- [44] S. A. Bass, C. Hartnack, Stocker, H. Stocker, W. Greiner, *Phys. Rev. C* **51**, 12 (R) (1995).
- [45] B. W. Barker, P. Danielewicz, *AIP Conf. Proc.* **1231**, 167 (2010).
- [46] M. Barranco and J. Treiner, *Nucl. Phys. A* **351**, 269 (1981).
- [47] M. Rashdan, A. Faessler, M. Ismail and N. Ohtsuka, *Nucl. Phys. A* **468**, 168 (1987).

- [48] R. Kubo, Rep. Prog. Phys. **29**, 255 (1966).
- [49] S. Piantelli *et al.* (INDRA Collaboration), Phys. Lett. **B627**, 18 (2005).
- [50] M. Parlog *et al.*, Eur. Phys. J. A **25**, 223 (2005).
- [51] Y. G. Ma, Q. M. Su, W. Q. Shen, J.S. Wang, D. Q. Fang, X.Z. Cai, H. Y. Zhang, D.D. Han, Eur. Phys. J. A **4**, 217 (1999).
- [52] D. Bandyopadhyaya, C. Samantaa, S.K. Samaddara and J.N. De, Nucl. Phys. A **511**, 1 (1990).
- [53] J. N. De, S. Das Gupta, S. Shlomo, and S. K. Samaddar, Phys. Rev. C **55**, R1641 (1997).